Journal of Magnetic Resonance 204 (2010) 111–117

Contents lists available at ScienceDirect

Journal of Magnetic Resonance

journal homepage: www.elsevier.com/locate/jmr

BEST-HNN and 2D-(HN)**NH** experiments for rapid backbone assignment in proteins

Dinesh Kumar [a], Subhradip Paul [a], Ramakrishna V. Hosur [a,b,*]

[a] Department of Chemical Sciences, Tata Institute of Fundamental Research, Homi Bhabha Road, Colaba, Mumbai 400005, India
[b] UM-DAE Centre for Excellence in Basic Sciences, Mumbai University Campus, Kalina, Santa Cruz, Mumbai 400098, India

ARTICLE INFO

Article history:
Received 27 November 2009
Revised 7 February 2010
Available online 20 February 2010

Keywords:
Fast acquisition
Longitudinal relaxation enhancement
Resonance assignment
Band selective excitation
HNN

ABSTRACT

HNN has proven to be an extremely valuable experiment for rapid and unambiguous backbone (H^N, ^{15}N) assignment in (^{13}C, ^{15}N) labeled proteins. However, low sensitivity of the experiment is often a limiting factor, especially when the transverse relaxation times (T_2) are short. We show here that BEST modification Schanda et al. (2006) [2] increases the sensitivity per unit time by more than a factor of 2.0 and thus substantially increases the speed of data collection; good 3D data can be collected in 8–10 h. Next, we present a simple method for amino-acid type identification based on simple 2D versions of the HNN experiment, labeled here as 2D-(HN)**NH**. Each of these experiments which produce anchor points for Gly, Ala, Ser/Thr residues, can be recorded in less than an hour. These enable rapid data acquisition, rapid analysis, and consequently rapid assignment of backbone (H^N, ^{15}N) resonances. The 2D-(HN)**NH** experiment does not involve aliphatic/aromatic protons and hence can be applied to deuterated protein samples as well, which is an additional advantage. The experiments have been demonstrated with human ubiquitin (76 aa) and acetic-acid denatured HIV-1 protease (99 aa), as representatives of folded and unfolded protein systems, respectively.

1. Introduction

The first and the key step of NMR[1] study of a protein is 'backbone assignment'. Getting this information rapidly is a further demand in structural genomics research. With this view methodological developments are occurring continuously, and many new pulse sequences have been published to save on experimental time [1–8]. HNN and HN(C)N experiments [9] published few years ago have proven extremely useful in this regard [9–15]. Compared to the other methods routinely used for backbone assignment, the main strength HNN and HN(C)N experiments [9] lies in the fact that the various planes in the 3D HNN and HN(C)N spectra contain positive and negative peaks. The patterns of these positive and negative peaks, which connect triplets of residues, depend upon the nature of the residues in the triplet sequences [9,11–14]. These are called triplet fixed points along the polypeptide chain. There are variants of the basic experiments [9–11,14], which generate special patterns around glycines, alanines, and serines/threonines. This advantage of HNN and HN(C)N is in addition to the fact that they provide direct correlations in the ^{15}N plane of a particular residue to its neighboring residues (i.e. the amide group of residue i shows correlation with the amide nitrogen of residues $i+1$ and $i-1$). These unique features make the assignment process extremely fast and unambiguous. The utility of these experiments can be enhanced further, if the information contained in them can be extracted faster by (i) enhancing the sensitivity of the experiments, (ii) reducing the time taken to record these spectra and/or (iii) designing 2D variants which can be recorded much faster to achieve the same purpose. The present paper describes our efforts in that direction for the HNN experiment.

We first describe a simple modification incorporating the BEST NMR concept [2,16] which substantially increases the sensitivity per unit time and thus the speed of data collection; good 3D data can be collected in 8–10 h. Next, we present a simple method for amino-acid type identification based on 2D versions of the 3D HNN experiment, labeled here as 2D-(HN)**NH**; this is basically the projection down the F_1 axis of the 3D HNN spectrum. The three variants of the experiment [2D-(HN)**NH-G**, 2D-(HN)**NH-A**, and 2D-(HN)**NH-ST**)] produce sufficient start/anchor points for Gly, Ala, Ser/ Thr residues which in turn will aid the assignment process; each of these can be recorded in less than an hour. Several methods have also been introduced earlier for identifying amino acid types in the NMR spectra [17–24]. These include side chain based methods [17–20], 2D-(HC)**NH** [25], MUSIC sequences [23,24], HADAMAC method [22] and the method proposed by Barnwal et al. [21] which is based on using combination of chemical shifts [21].

* Corresponding author. Address: Department of Chemical Sciences, Tata Institute of Fundamental Research (TIFR), Homi Bhabha Road, Colaba, Mumbai 400005, India. Fax: +91 22 22804610.
E-mail address: hosur@tifr.res.in (R.V. Hosur).

[1] *Abbreviations used:* NMR, nuclear magnetic resonance; HSQC, heteronuclear single quantum correlation; BEST, band-selective excitation short-transient; TE, transfer efficiency.

1090-7807/$ - see front matter © 2010 Elsevier Inc. All rights reserved.
doi:10.1016/j.jmr.2010.02.013

However, the main advantage of the method proposed here lies in the fact that 2D-(HN)**NH** experiment is applicable to deuterated proteins as well. Also, its experimental implementation is much simpler.

We envisage that a combination of the two developments described above, namely, strategy based on variants of 2D-(HN)**NH** and BEST modifications thereof, will contribute to several fold enhancement in the speed of backbone assignment. The experimental benefits have been demonstrated with human ubiquitin (76 aa) and acetic-acid denatured HIV-1 protease (99 aa), as representative of folded and unfolded protein systems. The modifications with regard to the HN(C)N pulse sequence, which, in principle, would be very similar to those in HNN will, however, be presented separately for purposes of greater focus and clarity.

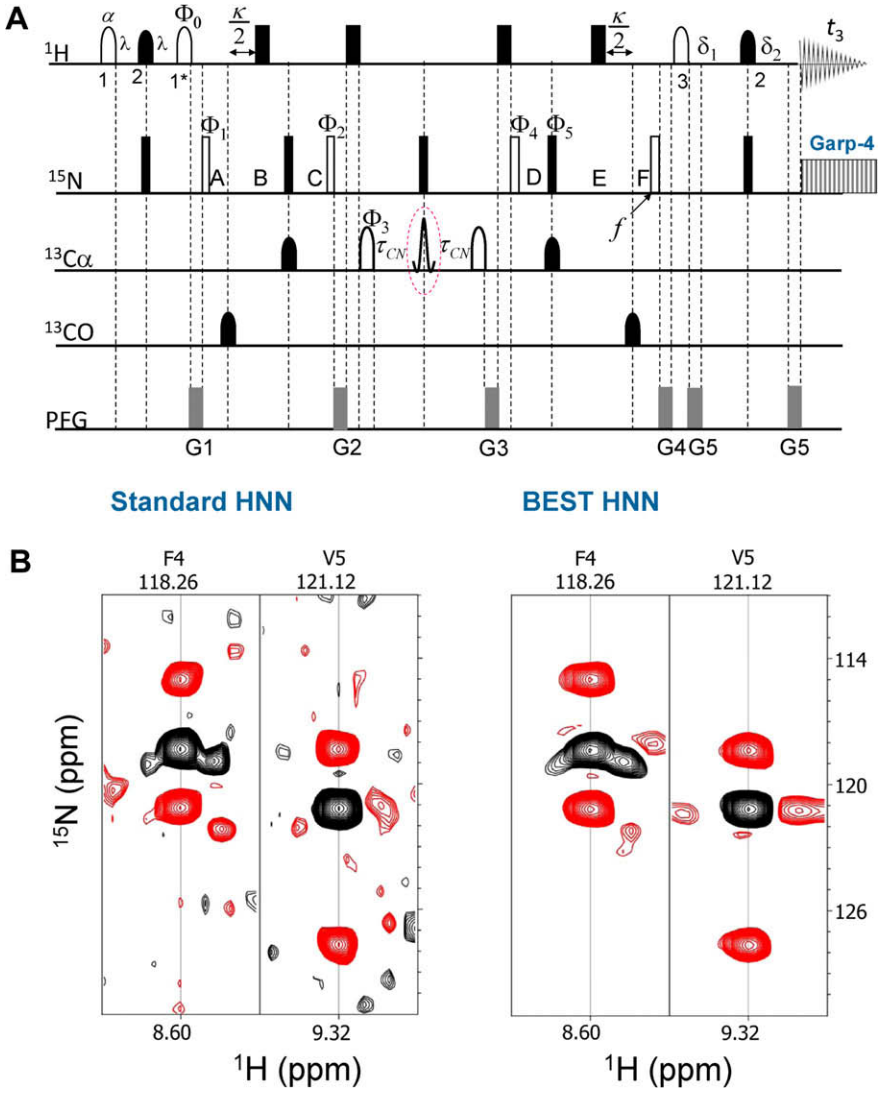

Fig. 1. (A) BEST_HNN pulse sequence. The details of the pulse sequence are the same as in reference [14], but for the following modifications: shaped pulses on proton channel indicate selective ^{1}H pulses, which are centered at 8.2 ppm, covering a bandwidth of 4.0 ppm (~6–10 ppm). The shaped pulses 1, 2, and 3 in the figure represent PC9 [30,34], REBURP [28], and EBURP2 [28], respectively. The pulse labeled 1^* is a flip back pulse obtained by time and phase reversal. The flip angle α of the first pulse has to be optimized and we have used a value of 100°. At 800 MHz, the duration of these pulses are respectively, 2.25, 1.5, and 1.44 ms. Filled rectangular pulses on ^{1}H channel indicate BIP-720-50-20 pulses (200 μs) [35] applied for ^{1}H decoupling during most of the t_1 and t_2 evolution periods, while ^{15}N decoupling during acquisition is obtained using the GARP-4 sequence with the field strength of 0.7 kHz. The ^{13}C carrier frequency for pulses, respectively, on ^{13}Cα and ^{13}CO channels are set at 56.0 and 176.0 ppm, except for the encircled pulse on carbon channel, where it is set as per the HNN variant (see Table 1). The strength of the ^{13}Cα pulses (standard Gaussian cascade Q3 (180°) and Q5 (90°) pulses) is adjusted so that they cause minimal excitation of carbonyl carbons. The band-selective 180° pulse – responsible for tunability of HNN – is encircled for emphasis. The 180° ^{13}CO shaped pulse (width 200 μs) had a standard Gaussian cascade Q3 pulse profile with minimal excitation of $^{13}C^{\alpha}$. For PC9, REBURP, and EBURP pulses, chemical shift and J_{NH}-coupling evolution remains active during ~50% of the pulse length. Thus, the delays used here are set to $\lambda = 2.5 - (2.25 \times 0.5) - (1.5 \times 0.5)$ ms = 625 μs, $\kappa = 5.4$ ms, $\delta_1 = 2.5 - (1.44 \times 0.5) - (1.5 \times 0.5)$ ms = 1.03 ms, and $\delta_1 = 2.5 - (1.5 \times 0.5)$ ms = 1.75 ms. The τ_{CN} must be optimized and is around 12–14 ms. The delays in the constant time periods are: $A = t_1/2$, $B = T_N$, $C = T_N - t_1/2$, $D = T_N - t_2/2$, $E = T_N$, and $F = t_2/2$. The value of T_N is 14 ms. The phase cycles are: $\Phi_1 = 2(x), 2(-x)$; $\Phi_2 = \Phi_3 = x, -x$; $\Phi_4 = 4(x), 4(-x)$; $\Phi_5 = x$, and $\Phi_{receiver} = 2(x), 4(-x), 2(x)$. Frequency discrimination in t_1 and t_2 has been achieved using States-TPPI phase cycling of Φ_1 and Φ_5, respectively, along with the receiver phase. The gradient (smoothed square shaped, SMSQ10.100) levels are as follows: $G_1 = 30\%$ (1 ms), $G_2 = 30\%$ (1 ms), $G_3 = 30\%$ (1 ms), $G_4 = 50\%$ (1 ms), and $G_5 = 80\%$ (500 μs) of the maximum strength of 53 G/cm along the z-direction. (B) $F_1(^{15}N) - F_3(H^N)$ strips of the standard and BEST_HNN spectra for residues F4–V5 in ubiquitin to depict a sensitivity comparison. Both the spectra were recorded on a Bruker 800 MHz spectrometer at 25 °C in the same amount of time (~9 h 1 min) using 512 complex points in the direct dimension, 32 complex points in the indirect dimensions and an inter-scan relaxation delay of 300 ms. The spectra plotted at the same contour levels clearly depict higher sensitivity in BEST_HNN compared to that in the normal HNN. The $F_2(^{15}N)$ values – which help to identify diagonal peaks – and the corresponding residues are indicated at the top for each strip. The black and red contours indicate positive and negative peaks, respectively. The residues corresponding to diagonal peaks in each strip have been shown at the top of each strip. (For interpretation of the references to colour in this figure legend, the reader is referred to the web version of this article.)

Table 1
Tuning of HNN experiment by making the encircled pulse in HNN pulse sequence selective according to the information required.

Type of BEST experiment	Encircled pulse in Fig. 1	Optimum offset (ppm)	Optimum excitation band-width (ppm)
HNN-G or normal HNN	Gaussian cascade Q3 pulse	45	80 (5–85 ppm range)
HNN-A	Gaussian cascade Q3 pulse	50	60 (20–80 ppm range)
HNN-S/T	Gaussian cascade Q3 pulse	64	32 (48–80 ppm range)

2. Materials and methods

The BEST_HNN pulse sequences for obtaining sequential connectivities were tested on 1.6 mM uniformly $^{15}N/^{13}C$ labeled human ubiquitin dissolved in phosphate buffer pH 6.5 in 90% H_2O and 10% D_2O (a product from Cambridge Isotope Laboratories, Inc.). All NMR experiments were performed at 25 °C on a Bruker Avance III spectrometer equipped with a cryoprobe, operating at ^1H frequency of 800 MHz. For BEST_HNN experiment, the delays $2T_N$, and $2\tau_{CN}$ were set to 28 and 24 ms, respectively (see Ref. [9] for description of these delays). For 3D experiments, 1024 complex points were collected along the direct dimension while 32 complex points were used along both the indirect dimensions. The relaxation delay and the number of scans per FID used were, respectively, 300 ms and 16. For 2D experiments, 1024 complex points were collected along the direct dimension while 64 complex points were used along both the indirect dimensions. The relaxation delay and the number of scans per FID used were, respectively, 200 ms and 80. The acquisition time for 3D and 2D experiments were approximately 9 h 1 min and 1 h 7 min, respectively. The variants of 2D-(HN)**NH** experiments in case of HIV-1 protease were recorded with 1024 complex points in direct dimension and 58 complex points along the indirect dimension [the shorter ^{15}N spectral width (22 ppm) does not allow to acquire higher number of increments]. The relaxation delay and number of scans per FID used were 1 s and 128, respectively. The acquisition time per variant was ~2 h, 10 min. The data was processed on Bruker software Topspin 2.1 (http://www.bruker.com/) and analyzed using CARA [26]. For the variants of the HNN and 2D-(HN)**NH** experiments [9,11,14] the parameters for the band selective $C^{\alpha/\beta}$ inversion pulse (encircled pulse in Fig. 1, which in this case is Gaussian cascade Q3 pulse [27]) are shown in Table 1.

3. Results and discussions

Fig. 1A shows the BEST modification of the HNN pulse sequence. The BEST strategy [2,16] employs selective excitation of the amide region (indicated by shaped pulses), and the relaxation delay is substantially reduced which saves on data acquisition time. The initial ^1H–^{15}N INEPT-transfer step requires an excitation, a refocusing, and a flip back pulse. For refocusing, a REBURP shape [28] was used because of its clean off-resonance performance resulting in less perturbation of the aliphatic ^1H spin polarization and, as a consequence, shorter longitudinal relaxation times of the amide proton spins. In order to minimize ^1H transverse relaxation delays, PC9 pulses were used for excitation and flip back. The PC9 pulses have been shown to perform well for a whole range of flip angles and provide the desired "top-hat" excitation profile for flip angles $0° < \alpha < 120°$) [29,30]. For the present application, the flip angle for the first PC9 pulse (i.e. α) is optimized for best excitation of the amide protons. At the end of the N → C transfer delay ($2T_N$), ^{15}N–^1H INEPT-transfer was achieved using EBURP-2 pulse shape [28] for the 90° rotation and REBURP shape for refocusing. All these pulses (PC9, REBURP, and EBURP-2) allow chemical shift and J_{NH}-coupling evolution during ~50% of their respective pulse lengths. This allows shortening the subsequent transfer delays: λ, δ_1, and δ_2 as shown in Fig. 1A. More details about the use of these shaped pulses for BEST NMR experiments can be found in references [2,31].

The coherence transfer pathway of the BEST_HNN experiment (Fig. 1A) is identical to the corresponding hard-pulse based HNN experiment [9,11,13,14] and employs the following pathway:

$$H_i^N \xrightarrow{k} N_i(t_1) \xrightarrow{2T_N} C^{\alpha}_{i-1,i} \xrightarrow{2\tau_{CN}} N_{i-1,i,i+1}(t_2) \xrightarrow{2T_N} H_{i-1,i,i+1}(t_3)$$

The delays $2T_N$ and $2\tau_{CN}$ are the time periods during which magnetization transfers take place. Among the various evolutions through the pulse sequence, the evolution during the $2\tau_{CN}$ period is the most crucial from the sensitivity point of view, as, it is this period during which magnetization resides on the C^{α} carbon which has the highest transverse relaxation rate, and its optimization is crucial for best sensitivity; it turns out that a value in the range 24–28 ms seems to be good choice. The C^{α} evolution during $2\tau_{CN}$ has another important consequence; it is accompanied by $C^{\alpha} - C^{\beta}$ coupling evolution which is precisely the basis of generation of glycine dependent peak patterns in the planes of the 3D spectrum; more details about the HNN pulse sequence can be found in references [9,11,13,14]. Note that, for a given protein, the bandwidth and carrier frequency of the pulses on proton channel need to be adjusted to cover the complete but only the amide proton chemical shift region, with minimal perturbation of water and aliphatic region. Amide ^1H chemical shifts at the edge of the excitation bandwidth will result in weak cross peaks.

The BEST_HNN experiment was tested on 1.6 mM ubiquitin and all the expected correlation peaks were observed. Fig. 1B shows a comparison of the selected strips from HNN and BEST-HNN spectra

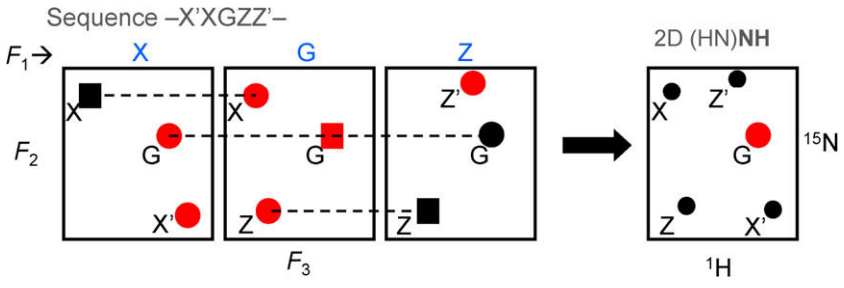

Fig. 2. Schematic to explain how an HSQC spectrum is obtained in 2D-(HN)**NH** experiment for a polypeptide sequence, X′XGZZ′, where G represents glycine and X′, X, Z, and Z′ represent any residue other than glycine. The panels on the left are F_3–F_2 planes through the HNN spectrum at the F_1 chemical shifts of residues indicated at the top. Black and red colors in the schematic represent positive and negative signs, respectively. Squares and circles represent the self and sequential peaks, respectively. The right most panel represents F_1 projection of all the planes that will be observed in the 2D-(HN)**NH** spectrum. The final sign of any peak upon summation of all the peaks from the three sequentially connected planes depends on the relative intensities of the individual peaks. It has been found that the self peak, in fact, dominates. Big and small circles are used to indicate differences in intensities.

of ubiquitin recorded with identical delay parameters and in the same amount of time (~9 h 1 min). The spectra have been plotted at the same contour levels. It is clearly seen that S/N in BEST_HNN is higher compared to that in normal HNN. The complete sequential walk through this spectrum for ubiquitin has been shown in Fig. S1. The sequence has also been tested successfully on a denatured protein, namely, denatured HIV-1 protease. Fig. S2 shows an illustrative sequential walk in this case.

Next, we present a method for amino-acid type identification based on 2D-(HN)**NH** experiment which is basically the projection down the F_1 axis of the 3D HNN spectrum. For better appreciation of the facts, we briefly repeat here some of the theoretical details of the three dimensional HNN experiment [9]. The HNN experiment displays, on its different 2D planes $^1H^N$ and ^{15}N correlations between three consecutive residues, $i-1$, i, and $i+1$; the peaks appear at the coordinates:

$$F_1 = N_i, (F_3, F_2) = (H_i, N_i),\ (H_{i-1}, N_{i-1}),\ (H_{i+1}, N_{i+1})$$
$$F_1 = N_i, (F_3, F_1) = (H_i, N_i),\ (H_i, N_{i-1}),\ (H_i, N_{i+1})$$

Thus, in each plane there occurs a diagonal peak $F_1 = F_2 = N_i$ for each residue and there are two sequential peaks to residues $(i-1)$ and $(i+1)$. In the $F_2 - F_3$ plane, the self and sequential peaks appear at their normal HSQC positions. Now, if there is no t_1 evolution (i.e. during time $2T_N = A + B + C$), all the self and sequential cross peaks for a residue will overlap and will result in a normal ^1H–^{15}N HQSC type spectrum, but the relative intensities will be resultant of the co-additions of the self and the sequential peaks (Fig. 2 (schematic) and Fig. 3 (theoretical)). As we show below, peaks from glycine residues appear negative in sign while those from all the other residues appear positive.

For a chain of four residues, $i-2$ to $i+1$, the intensities of the diagonal $\left(I_i^d\right)$ and the cross peaks $(I_{i-1}^c,\ I_{i+1}^c)$ in the (F_2, F_3) planes of the HNN spectrum are given by [9,11]:

$$I_i^d = -\left(E_1^2 E_3 E_9 K_{i,1}^d + E_2^2 E_5 E_{10} K_{i,2}^d\right) \tag{1}$$
$$I_{i-1}^c = E_1 E_4 E_7 E_9 K_{i-1}^c;\ I_{i+1}^c = E_2 E_6 E_8 E_{10} K_{i+1}^c; \tag{2}$$

where,

$$\begin{aligned}
E_1 &= \cos(p_i T_N)\sin(q_{i-1} T_N),\\
E_2 &= \sin(p_i T_N)\cos(q_{i-1} T_N),\\
E_3 &= \cos(p_{i-1}\tau_{CN})\cos(q_{i-1}\tau_{CN}),\\
E_4 &= \sin(p_{i-1}\tau_{CN})\sin(q_{i-1}\tau_{CN}),\\
E_5 &= \cos(p_i\tau_{CN})\cos(q_i\tau_{CN}),\\
E_6 &= \sin(p_i\tau_{CN})\sin(q_i\tau_{CN}),\\
E_7 &= \sin(p_{i-1} T_N)\cos(q_{i-2} T_N),\\
E_8 &= \cos(p_{i+1} T_N)\sin(q_i T_N),\\
E_9 &= \cos n_{i-1}\tau_{CN},\\
E_{10} &= \cos n_i\tau_{CN},
\end{aligned} \tag{3}$$

and

$$p_i = 2\pi {}^1J(C_i^\alpha\text{–}N_i);\ q_i = 2\pi {}^2J(C_i^\alpha\text{–}N_{i+1});$$
$$n_i = 2\pi {}^2J\left(C_i^\alpha - C_i^\beta\right), \tag{4}$$
$$K_{i,1}^d = \exp\left(-4T_N R_2^{N_i} - 2\tau_{CN} R_2^{C_{i-1}^\alpha}\right),$$
$$K_{i,2}^d = \exp\left(-4T_N R_2^{N_i} - 2\tau_{CN} R_2^{C_i^\alpha}\right),$$
$$K_{i-1}^c = \exp\left(-2T_N\left(R_2^{N_i} + R_2^{N_{i-1}}\right) - 2\tau_{CN} R_2^{C_{i-1}^\alpha}\right),$$
$$K_{i-1}^c = \exp\left(-2T_N\left(R_2^{N_i} + R_2^{N_{i+1}}\right) - 2\tau_{CN} R_2^{C_i^\alpha}\right), \tag{5}$$

Here in Eq. (4), ^1J, ^2J and are one-bond and two-bond coupling constants corresponding to the respective terms in brackets. The average value of one-bond or two-bond N–C^α coupling constant for the α and β types of structures are slightly different: [32] for α helices,

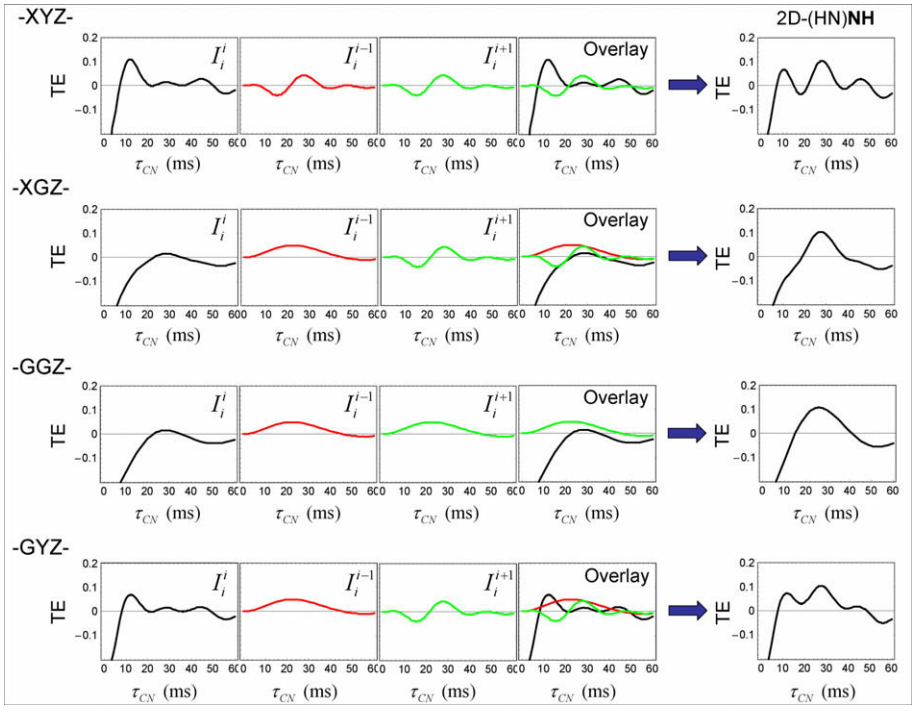

Fig. 3. Plots of coherence transfer efficiencies plotted as a function of. The plots were calculated for T_N value of 15.0 ms and values of $^1J_{C^\alpha C^\beta}$, $^1J_{C^\alpha N}$, and $^2J_{C^\alpha N}$ equal to 35, 11, and 7 Hz, respectively. The values of R_2^N, and $R_2^{C^\alpha}$ are 10 and 15 s^{-1}, respectively. From left to right, first four plots represent variation in peak intensity in the 3D HNN spectrum for the central residue in the triplet stretch shown in the figure; first plot shows intensity of self peak at its own plane, second plot shows peak intensity of residue it i at plane of residue $i-1$, third plot shows peak intensity of residue i at plane of residue $i+1$, and fourth plot shows overlay of all the previous three intensities. Right most panels represent variations in the peak intensities in the 2D-(HN)**NH** spectrum for the central residue in the triplet stretches.

$^1J_{C^\alpha-N}$ and $^2J_{C^\alpha-N}$ are in the ranges 8–10 and 4–6 Hz, respectively, and for β structures these values are in the ranges 10–13 and 6–9 Hz, respectively. Thus, based on the coupling constants, the delays $2T_N$, and $2\tau_{CN}$ become protein dependent and thus have to be optimized. A detailed analysis of Eq. (3) reveals that for the optimum choices of the transfer periods (12–14 ms) [9,11,14], the functions E_1 to E_8 are all positive whereas, E_9 and E_{10} remain negative ($\simeq$1.0). This means depending upon presence or absence of E_9 and E_{10} terms (which originate from evolution under C^α–C^β coupling during $2\tau_{CN}$ period) the cross peaks can have negative or positive signs, respectively. This is the basis of generation of different patterns of peaks due to glycines which do not have a C^β carbon. Consequently, either E_9 and E_{10} term will be absent, depending on whether glycine is present at i or $(i-1)$ position. For example, for glycine at position i and if $(i-1)$ is other than glycine (i.e. a triplet stretch of –XGZ– type), E_{10} term would be absent, then Eqs. (1) and (2) will get modified as below:

$$I_i^d = -\left(E_1^2E_3E_9K_{i,1}^d + E_2^2E_5K_{i,2}^d\right)$$
$$I_{i-1}^c = E_1E_4E_7E_9K_{i-1}^c;\ I_{i+1}^c = E_2E_6E_8K_{i+1}^c \quad (6)$$

For a triplet stretch of –GXZ– type; E_9 term would be absent, then Eqs. (1) and (2) will get modified as:

$$I_i^d = -\left(E_1^2E_3K_{i,1}^d + E_2^2E_5E_{10}K_{i,2}^d\right)$$
$$I_{i-1}^c = E_1E_4E_7K_{i-1}^c;\ I_{i+1}^c = E_2E_6E_8E_{10}K_{i+1}^c \quad (7)$$

Similarly, for a triplet stretch of –GGZ– type; both E_9 and E_{10} terms would be absent, then Eqs. (1) and (2) will get modified as:

$$I_i^d = -\left(E_1^2E_3K_{i,1}^d + E_2^2E_5K_{i,2}^d\right)$$
$$I_{i-1}^c = E_1E_4E_7K_{i-1}^c;\ I_{i+1}^c = E_2E_6E_8K_{i+1}^c \quad (8)$$

Now, consider the 2D-(HN)**NH** spectrum. Here, the intensity of each peak will be dictated by the following equation:

$$I_i^{2D} = I_i^i + I_i^{i-1} + I_i^{i+1} \quad (9)$$

where, I_i^i is the intensity of self peak at its own plane, I_i^{i-1} is the intensity of ith peak at plane of $i-1$ residue and I_i^{i+1} is the intensity of the ith peak in the plane of $i+1$ residue. Thus, for a triplet sequence of –XYZ– (where X, Y, and Z are any residue other than glycine and proline), intensity of peak for residue Y in 2D-(HN)**NH** spectrum will be;

$$I_i^{2D} = -\left(E_1^2E_3E_9K_{i,1}^d + E_2^2E_5E_{10}K_{i,2}^d\right) + E_1E_4E_7E_9K_{i-1}^c + E_2E_6E_8E_{10}K_{i+1}^c \quad (10)$$

For a triplet stretch of –GYZ– type, the intensity of peak for residue Y in 2D-(HN)**NH** spectrum will be:

$$I_i^{2D} = -\left(E_1^2E_3K_{i,1}^d + E_2^2E_5E_{10}K_{i,2}^d\right) + E_2E_6E_8K_{i+1}^c + E_1E_4E_7E_9K_{i-1}^c \quad (11)$$

For a triplet stretch of –XGZ– type, the intensity of peak for residue G in 2D-(HN)**NH** spectrum will be:

$$I_i^{2D} = -\left(E_1^2E_3E_9K_{i,1}^d + E_2^2E_5K_{i,2}^d\right) + E_2E_6E_8E_{10}K_{i+1}^c + E_1E_4E_7K_{i-1}^c \quad (12)$$

A glycine present at $i+1$ position does not change the peak pattern and hence will be equivalent to normal residue. For another case where glycines are present at two positions i and $i-1$ (i.e. a triplet stretch of –G′GX– type or –G′GG″–type), the intensity of peak for residue G in 2D-(HN)**NH** spectrum will be:

$$I_i^{2D} = -\left(E_1^2E_3K_{i,1}^d + E_2^2E_5K_{i,2}^d\right) + E_2E_6E_8K_{i+1}^c + E_1E_4E_7K_{i-1}^c \quad (13)$$

Thus considering different triplet of residues, covering the general and all the special situations, we explicitly calculated the peak intensities as a function of τ_{CN}, the most crucial adjustable parameter and these are shown in Fig. 3. The peak intensities were calculated for values of $^1J_{C^\alpha-N}$ and $^2J_{C^\alpha-N}$ equal to 11 and 7 Hz, respectively, under the assumption that all $^1J_{C^\alpha-N}$ and $^2J_{C^\alpha-N}$ have the same values. The calculations are shown with explicit inclusion of relaxation effects using typical relaxation parameters for a protein of this size. The calculation showed that the final sign of the peak in 2D-(HN)**NH** spectrum is dictated by I_i^i term in the Eqs. (10)–(13) (i.e. the sign of self peak on its own F_2–F_3 plane of 3D HNN spectrum). Moreover, the presence or absence or proline in the triplet stretch will not make any difference to the peak signs in the final spectrum, except that the intensity of the ith peak will increase when there is a proline at $i-1$ position. This 2D spectrum will, hereafter, be referred to as (HN)**NH-G**. Similar situations will arise for the HNN variants, namely, HNN-A [11] and HNN-S/T [14]; in the former alanines will also behave like glycines and in the latter serines/threonines will behave like glycines. These two experiments will hereafter br referred to as 2D (HN)**NH-A** and 2D-(HN)**NH-S/T**, respectively. All these 2D spectra can be recorded in less than an hour each from the respective 3D pulse sequences, by not incrementing the t_1 variable of the 3D experiment.

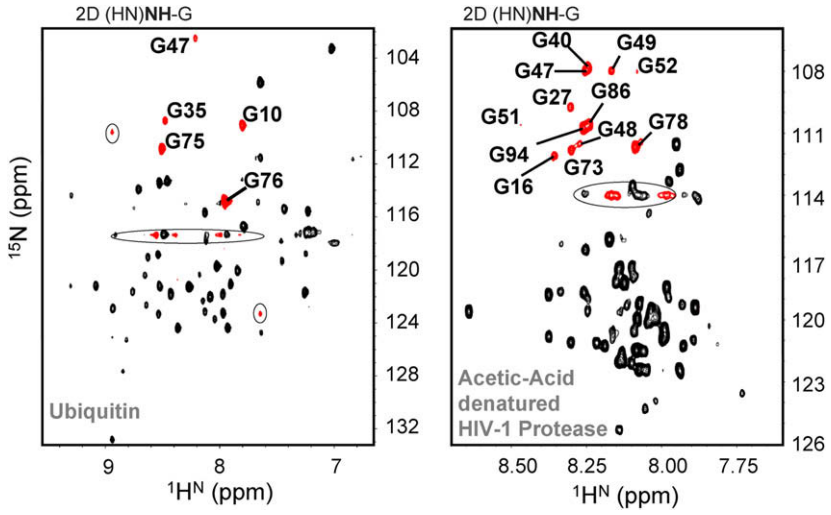

Fig. 4. The 2D-(HN)**NH-G** spectra for folded ubiquitin (left) and denatured HIV-1 protease (right) recorded on a 800 MHz Bruker spectrometer. The peaks encircled in both the spectra represent non-HSQC peaks coming from experimental artifacts.

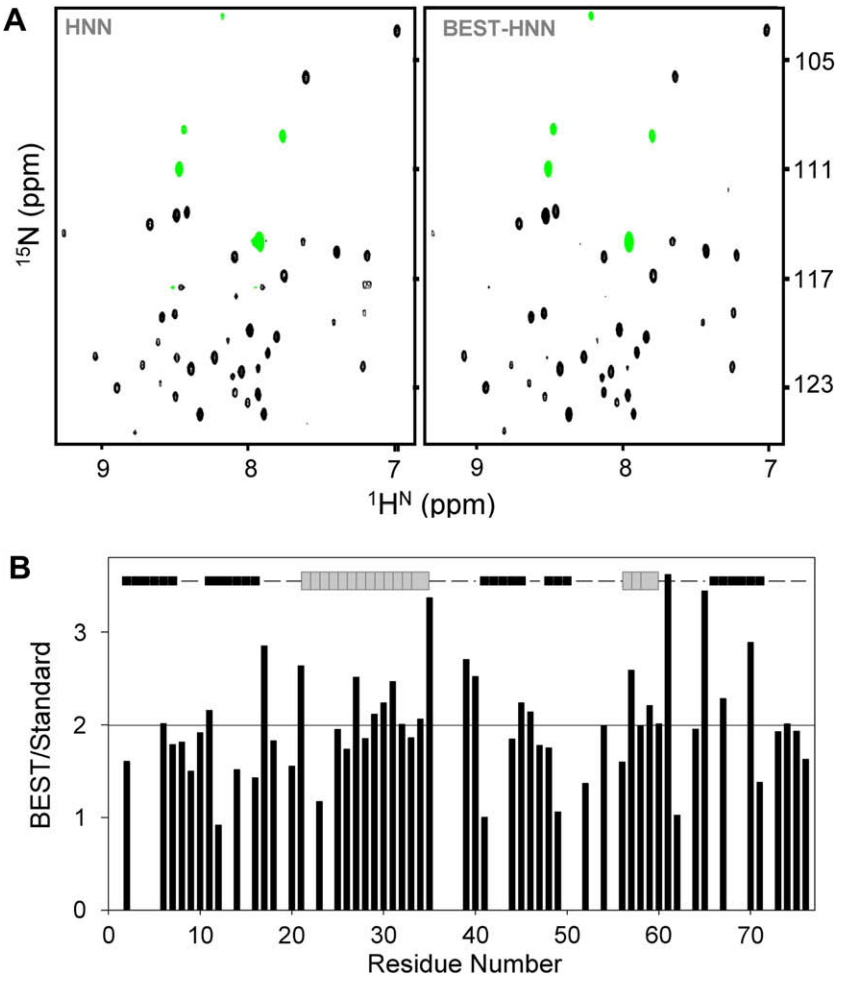

Fig. 5. (A) Comparison of spectral regions of standard (left) and BEST modified (right) 2D-(HN)**NH** spectra recorded on ubiquitin sample. For both the experiments, 512 complex points were recorded in ^{1}H dimension while 64 complex points were used in the ^{15}N dimension for spectral widths of 11 and 33 ppm, respectively, in proton and nitrogen dimensions. The inter-scan delay for both the experiments is 200 ms; number of scans per fid was 80. Acquisition time in each case was 1 h, 7 min. (B) Plot of intensity ratios for individual amide correlation peaks against residue number.

The variants of 2D-(HN)**NH** experiment have successfully been tested on folded ubiquitin (76 amino acid, BMRB Accession No.: 15410) and acetic-acid-denatured HIV-1 protease [33] (99 amino acid). Assignments are known in both the cases and thus they served as excellent test cases. Fig. 4 displays a section of the 2D-(HN)**NH-G** spectra of folded ubiquitin (left) and denatured HIV-1 protease (right). Results from the other two variants of 2D-(HN)**NH** have been included in the supplementary material (Fig. S3). Thus, glycines, alanines, and serine/threonines can be easily identified in the 2D-(HN)**NH** spectra.

Next, we show the sensitivity gain in the 2D versions of BEST _HNN presented here. Fig. 5A shows comparison of spectral regions of normal and BEST spectra, both recorded with an inter scan delay (t_{rec}) of 200 ms. The experimental time in each case was roughly the same (~1 h 7 min). Fig. 5B shows residue-wise intensity ratios (BEST/standard) from which it is clear that the intensities in the BEST spectra are significantly higher than those in the standard one; the gain factor is as much as ~3.6 in one case, the average gain being ~2.0.

To summarize, complete (H^{N}, ^{15}N) backbone assignments in (^{15}N, ^{13}C) labeled proteins can be obtained very rapidly, perhaps in less than a day, by recording one 3D BEST-HNN spectrum in about 8–10 h and a few variants of 2D-(HN)**NH** spectra which generate Gly, Ala, Ser/Thr labels in HSQC type displays. With BEST modification the 2D spectra can be recorded in less than half-an-hour each. The fact that the experiments have proven successful even for denatured HIV-1 protease, enhances the general applicability of the protocol. Thus, we anticipate that the protocol described here can be of immense value for research in protein NMR. The pulse sequences described here are available upon request (hosur@tifr.res.in) or can also be downloaded from this link http://www.tifr.res.in/~hosur/download.htm.

Acknowledgments

We thank Government of India for providing financial support to the National Facility for High Field NMR at Tata Institute of Fundamental Research, India. D.K. acknowledge Detlef Moskou for providing his kind assistance during implementation of BEST NMR.

Supplementary data

Supplementary data associated with this article can be found, in the online version, at doi:10.1016/j.jmr.2010.02.013.

References

[1] L. Frydman, T. Scherf, A. Lupulescu, The acquisition of multidimensional NMR spectra within a single scan, Proc. Natl. Acad. Sci. USA 99 (2002) 15858–15862.
[2] P. Schanda, M.H. Van, B. Brutscher, Speeding up three-dimensional protein NMR experiments to a few minutes, J. Am. Chem. Soc. 128 (2006) 9042–9043.

[3] H.S. Atreya, T. Szyperski, Rapid NMR data collection, Methods Enzymol. 394 (2005) 78–108.
[4] E. Kupce, R. Freeman, Projection–reconstruction technique for speeding up multidimensional NMR spectroscopy, J. Am. Chem. Soc. 126 (2004) 6429–6440.
[5] R. Freeman, E. Kupce, New methods for fast multidimensional NMR, J. Biomol. NMR 27 (2003) 101–113.
[6] E. Kupce, R. Freeman, Fast multi-dimensional Hadamard spectroscopy, J. Magn. Reson. 163 (2003) 56–63.
[7] E. Kupce, R. Freeman, Fast multi-dimensional NMR of proteins, J. Biomol. NMR 25 (2003) 349–354.
[8] S. Hiller, F. Fiorito, K. Wuthrich, G. Wider, Automated projection spectroscopy (APSY), Proc. Natl. Acad. Sci. USA 102 (2005) 10876–10881.
[9] S.C. Panchal, N.S. Bhavesh, R.V. Hosur, Improved 3D triple resonance experiments, HNN and HN(C)N, for HN and 15N sequential correlations in (13C, 15N) labeled proteins: application to unfolded proteins, J. Biomol. NMR 20 (2001) 135–147.
[10] D. Kumar, J. Chugh, R.V. Hosur, Generation of serine/threonine check points in HN(C)N spectra, J. Chem. Sci. 121 (2009) 955–964.
[11] A. Chatterjee, A. Kumar, R.V. Hosur, Alanine check points in HNN and HN(C)N spectra, J. Magn. Reson. 181 (2006) 21–28.
[12] A. Chatterjee, N.S. Bhavesh, S.C. Panchal, R.V. Hosur, A novel protocol based on HN(C)N for rapid resonance assignment in ((15)N, (13)C) labeled proteins: implications to structural genomics, Biochem. Biophys. Res. Commun. 293 (2002) 427–432.
[13] N.S. Bhavesh, S.C. Panchal, R.V. Hosur, An efficient high-throughput resonance assignment procedure for structural genomics and protein folding research by NMR, Biochemistry 40 (2001) 14727–14735.
[14] J. Chugh, D. Kumar, R.V. Hosur, Tuning the HNN experiment: generation of serine–threonine check points, J. Biomol. NMR 40 (2008) 145–152.
[15] N.S. Bhavesh, A. Chatterjee, S.C. Panchal, R.V. Hosur, Application of HN(C)N to rapid estimation of 1J(N–C(alpha)) coupling constants correlated to psi torsion angles in proteins: implication to structural genomics, Biochem. Biophys. Res. Commun. 311 (2003) 678–684.
[16] E. Lescop, P. Schanda, B. Brutscher, A set of BEST triple-resonance experiments for time-optimized protein resonance assignment, J. Magn. Reson. 187 (2007) 163–169.
[17] D. Pantoja-Uceda, J. Santoro, Amino acid type identification in NMR spectra of proteins via beta- and gamma-carbon edited experiments, J. Magn. Reson. 195 (2008) 187–195.
[18] V. Tugarinov, R. Muhandiram, A. Ayed, L.E. Kay, Four-dimensional NMR spectroscopy of a 723-residue protein: chemical shift assignments and secondary structure of malate synthase g, J. Am. Chem. Soc. 124 (2002) 10025–10035.
[19] V. Dotsch, R.E. Oswald, G. Wagner, Selective identification of threonine, valine, and isoleucine sequential connectivities with a TVI-CBCACONH experiment, J. Magn. Reson. B 110 (1996) 304–308.
[20] V. Dotsch, H. Matsuo, G. Wagner, Amino-acid-type identification for deuterated proteins with a b-carbon-edited HNCOCACB experiment, J. Magn. Reson. B 112 (1996) 95–100.
[21] R.P. Barnwal, A.K. Rout, H.S. Atreya, K.V. Chary, Identification of C-terminal neighbours of amino acid residues without an aliphatic 13C gamma as an aid to NMR assignments in proteins, J. Biomol. NMR 41 (2008) 191–197.
[22] E. Lescop, R. Rasia, B. Brutscher, Hadamard amino-acid-type edited NMR experiment for fast protein resonance assignment, J. Am. Chem. Soc. 130 (2008) 5014–5015.
[23] M. Schubert, H. Oschkinat, P. Schmieder, MUSIC and aromatic residues: amino acid type-selective (1)H–(15)N correlations, III, J. Magn. Reson. 153 (2001) 186–192.
[24] M. Schubert, H. Oschkinat, P. Schmieder, MUSIC, selective pulses, and tuned delays: amino acid type-selective (1)H–(15)N correlations, II, J. Magn. Reson. 148 (2001) 61–72.
[25] J. Chugh, R.V. Hosur, Spectroscopic labeling of A, S/T in the 1H–15N HSQC spectrum of uniformly (15N–13C) labeled proteins, J. Magn. Reson. 194 (2008) 289–294.
[26] R. Keller, The Computer Aided Resonance Assignment Tutorial CANTINA, Verlag, Goldau, Switzerland, 2004.
[27] L. Emsley, G. Bodenhausen, Gaussian pulse cascades: new analytical functions for rectangular selective inversion and in-phase excitation in NMR, Chem. Phys. Lett. 165 (1990) 469–476.
[28] H. Geen, R. Freeman, Band-selective radiofrequency pulses, J. Magn. Reson. 93 (1991) 93–141.
[29] E. Kupce, R. Freeman, Wideband excitation with polychromatic pulses, J. Magn. Reson. A 108 (1994) 268–273.
[30] E. Kupce, R. Freeman, Polychromatic selective pulses, J. Magn. Reson. A 102 (1993) 122–126.
[31] P. Schanda, E. Kupce, B. Brutscher, SOFAST-HMQC experiments for recording two-dimensional heteronuclear correlation spectra of proteins within a few seconds, J. Biomol. NMR 33 (2005) 199–211.
[32] J. Wirmer, H. Schwalbe, Angular dependence of 1J(Ni, Calphai) and 2J(Ni, Calpha(i − 1)) coupling constants measured in J-modulated HSQCs, J. Biomol. NMR 23 (2002) 47–55.
[33] M.K. Rout, R.V. Hosur, Fluctuating partially native-like topologies in the acid denatured ensemble of autolysis resistant HIV-1 protease, Arch. Biochem. Biophys. 482 (2009) 33–41.
[34] E. Kupce, R. Freeman, Band-selective correlation spectroscopy, J. Magn. Reson. A 112 (1995) 134–137.
[35] M.A. Smith, A.J. Shaka, H. Hu, Improved broadband inversion performance for NMR in liquids, J. Magn. Reson. 151 (2001) 269–283.